

A prescription and fast code for the long-term evolution of star clusters – II. Unbalanced and core evolution

Mark Gieles¹, Poul E.R. Alexander², Henny J.G.L.M. Lamers³ and Holger Baumgardt⁴

¹ *Department of Physics, University of Surrey, Guildford, GU2 7XH, UK*

² *Institute of Astronomy, University of Cambridge, Madingley Road, Cambridge, CB3 0HA, UK*

³ *Astronomical Institute Anton Pannekoek, University of Amsterdam, PO Box 94249, 1090 GE Amsterdam, The Netherlands*

⁴ *School of Mathematics and Physics, University of Queensland, St. Lucia, QLD 4072, Brisbane, Australia*

Accepted 2013 October 9. Received 2013 October 8; in original form 2013 September 3

ABSTRACT

We introduce version two of the fast star cluster evolution code Evolve Me A Cluster of Stars (EMACSS). The first version (Alexander and Gieles) assumed that cluster evolution is balanced for the majority of the life-cycle, meaning that the rate of energy generation in the core of the cluster equals the diffusion rate of energy by two-body relaxation, which makes the code suitable for modelling clusters in weak tidal fields. In this new version, we extend the model to include an unbalanced phase of evolution to describe the pre-collapse evolution and the accompanying escape rate such that clusters in strong tidal fields can also be modelled. We also add a prescription for the evolution of the core radius and density and a related cluster concentration parameter. The model simultaneously solves a series of first-order ordinary differential equations for the rate of change of the core radius, half-mass radius and the number of member stars N . About two thousand integration steps in time are required to solve for the entire evolution of a star cluster and this number is approximately independent of N . We compare the model to the variation of these parameters following from a series of direct N -body calculations of single-mass clusters and find good agreement in the evolution of all parameters. Relevant time-scales, such as the total lifetimes and core collapse times, are reproduced with an accuracy of about 10% for clusters with various initial half-mass radii (relative to their Jacobi radii) and a range of different initial N up to $N = 65\,536$. The current version of EMACSS contains the basic physics that allows us to evolve several cluster properties for single-mass clusters in a simple and fast way. We intend to extend this framework to include more realistic initial conditions, such as a stellar mass spectrum and mass-loss from stars. The EMACSS code can be used in star cluster population studies and in models that consider the co-evolution of (globular) star clusters and large scale structures.

Key words: methods: numerical – star clusters: general – globular clusters: general – stars: kinematics and dynamics – Galaxy: kinematics and dynamics – open clusters and associations: general

1 INTRODUCTION

The dynamical evolution of star clusters is the result of several internal and external processes, including two-body relaxation, interactions between single and binary stars, escape across the tidal boundary and the internal evolution and mass-loss of single and binary stars (e.g. Meylan & Heggie 1997). Modelling collisional systems is challenging because all these effects operate on their own time-scale, ranging over many orders of magnitudes from the orbital period of hard binary stars to the Galactic orbit of the cluster, and depending in different ways on the number of stars N (Aarseth & Heggie 1998). The direct N -body approach is a versatile method for solving the gravitational N -body problem and correctly combines the interplay between the various dynamical scaling laws

and their corresponding time-scales. Owing to recent progress in the use of special hardware to accelerate the force calculations (Gaburov et al. 2009; Nitadori & Aarseth 2012) it is now feasible to model medium sized globular clusters ($N \simeq 2 - 3 \times 10^5$), with moderate initial densities, over a Hubble (Hurley & Shara 2012; Sippel & Hurley 2013). However, the $\mathcal{O}(N^2)$ nature of the computational effort of direct N -body integrations does not allow us yet to model globular clusters containing the number of stars of typical globular clusters (about 10^6) with realistic initial density ($\gtrsim 10^4 M_{\odot} \text{pc}^{-3}$) over a Hubble time

We aim to develop a relatively simple, and extremely fast (compared to the direct N -body approach) prescription for the evolution of a few fundamental properties of tidally limited clusters,

such as N and the various cluster radii (core radius, half-mass radius and tidal radius) with an N -independent computational effort. Having a fast and simplified prescription of complex astrophysical objects allows us to use these objects in population synthesis studies, or to combine the evolutionary prescription with that of other astrophysical phenomena. Examples exist for other applications, for example, for the evolution of individual stars of different mass and metallicity (Hurley et al. 2000), binary stars (Hurley et al. 2002), binary populations (Eldridge, Izzard & Tout 2008) and for the products of stellar collisions (Lombardi et al. 2002). A possible application of such a tool for star cluster evolution is the modelling of observed properties of star cluster populations (Jordán et al. 2005, 2007; Harris et al. 2013), which will enable us to use star clusters more efficiently as tracers of the formation and evolution of the host galaxy (Freeman & Bland-Hawthorn 2002; Brodie & Strader 2006; Prieto & Gnedin 2008; Gnedin, Ostriker & Tremaine 2013). Additionally, a fast prescription of cluster evolution can be combined with models of galaxy evolution or cosmology. Both applications are currently out of reach because existing, more sophisticated, methods to solve the N -body problem are computationally too expensive (for a review see the supplementary material of Portegies Zwart et al. 2010).

Gieles et al. (2011) present a simple analytical theory for the evolution of N and half-mass radius of tidally limited clusters. The model assumes that there is always a balance between the rate of energy generation in the core and the flux of energy through the half-mass radius by two-body relaxation. The theory connects two existing models of Michel Hénon: the isolated cluster (Hénon 1965) and the tidally limited cluster (Hénon 1961). To connect these models it was assumed that the energy conduction rate is the same in both models (for a derivation and comparison of these quantities see Gieles et al. 2011). Numerical N -body simulations recently confirmed the validity of this assumption (Alexander & Gieles 2012, hereafter Paper I).

In Paper I we present the first version of a versatile cluster evolution package in the form of the publicly available code Evolve Me A Cluster of StarS (EMACSS)¹. It allows a user to define the cluster and tidal field parameters and the code provides the evolution of cluster parameters based on the assumption of balanced evolution. The evolution of the number of stars N and half-mass radius r_h of a cluster are obtained by solving two coupled first-order ordinary differential equations, namely $\dot{N}(N, r_h, \Omega)$ and $\dot{r}_h(N, r_h, \Omega)$ with a fourth-order Runge-Kutta integrator. Here Ω is the angular frequency of the cluster about the centre of the galaxy. Several assumptions had to be made to reduce the evolution of clusters to such a simple model: relaxation driven escape of stars is the only mechanism that reduces N ; the cluster evolves in a self-similar fashion, such that r_h is a constant times the virial radius r_v (in this case $r_h = r_v$); cluster orbits are circular and the balanced evolution starts after a fixed number of initial half-mass relaxation time-scales τ_{rh} and the cluster is not evolved in that first phase.

This paper extends EMACSS to include the following physical processes: the evolution of the core radius r_c and core density ρ_c , the evolution of N and the radii in the unbalanced evolution phase prior to core collapse and the evolution of the ratio r_h/r_v . The last ratio depends on the density profile and therefore the concentration of the cluster. With these new additions, EMACSS can also evolve clusters that are initially filling the Roche volume and lose a large

fraction of their stars prior to core collapse. In the current version we assume that all stars have the same mass.

The structure of the paper is as follows: in Section 2 we introduce the theoretical framework of the new version of EMACSS. In Section 3 we present a suite of direct N -body simulations that is compared to EMACSS and used to implement the new features. In Section 4 we demonstrate the performance of EMACSS by comparing it to all N -body models and in Section 5 we present our conclusions and discuss the future steps for EMACSS that will include a stellar mass function and the mass-loss of stars.

2 FRAMEWORK

In this section, we set out the theoretical framework that is used to describe the evolution of the core radius r_c and core density ρ_c in the unbalanced phase (Section 2.2), the evolution of the other parameters in the unbalanced phase (Section 2.3) and the transition to the balanced phase and the evolution of the core (Section 2.4). The evolution of the half-mass radius in balanced evolution and the escape rates in both the balanced phase and the unbalanced phase are discussed in Sections 2.5 and 2.6, respectively. We start by introducing in Section 2.1 the variables, time-scales and definitions used in this paper.

2.1 Variables, definitions and time-scales

A fundamental aspect of the evolution of a collisional system, i.e. a star cluster, is the increase of the total energy (the system becoming less bound) on a time-scale shorter than the age of the Universe, because of two-body relaxation. For clusters in weak tidal fields, this energy increase (i.e. less negative) results in an expansion of the cluster and for tidally limited clusters the energy increase results in the escape of stars. The quantity we want to evolve in a cluster model is, therefore, the total energy E of the cluster (Gieles et al. 2011; Paper I). For a self-gravitating system in virial equilibrium E can be written as

$$E = -\kappa \frac{GM^2}{r_h}. \quad (1)$$

Here, G is the gravitational constant, M and r_h are the mass and the half-mass radius of the cluster, respectively, and κ is a form-factor that depends on the density profile of the cluster. In the definition of E , we do not include the binding energy of multiple stars. This definition of E is often referred to as the *external* energy (as in Giersz & Heggie 1997). We assume that the only contributions to the total energy are the kinetic energy T and the gravitational energy W , such that $E = T + W = W/2 = -T$. Combined with the definition of the virial radius $r_v = -GM^2/(2W)$ we then find that $\kappa = r_h/(4r_v)$. Note that we ignore the contribution of the tidal field E_{tide} to the total energy. Fukushima & Heggie (1995) show that the ratio $E_{\text{tide}}/W \simeq 0.4(r_h/r_J)^3$ for a tidal field due to a point-mass galaxy, which even for very large ratios of r_h/r_J results in a relative contribution of E_{tide} to E of only a few percent. We do include the effect the tides have on the escape of stars.

Taking the time-derivative on each side of equation (1) and dividing by $-E$ we find how the fractional change in energy relates to the fractional change in the other variables

$$-\frac{\dot{E}}{E} = -\frac{\dot{\kappa}}{\kappa} + \frac{\dot{r}_h}{r_h} - 2\frac{\dot{m}}{m} - 2\frac{\dot{N}}{N}. \quad (2)$$

Here we have used $M = mN$, where m is the mean mass of the

¹ The code is available from <http://github.com/emacss>

stars and N is the number of stars. In this work we assume single-mass clusters so $\dot{m} = 0$ from now on². We are interested in the evolution of these quantities on a half-mass relaxation time-scale τ_{rh} which is defined as (Spitzer & Hart 1971)

$$\tau_{\text{rh}} = 0.138 \frac{N^{1/2} r_{\text{h}}^{3/2}}{\sqrt{Gm \ln(0.11N)}}. \quad (3)$$

Here $\ln(0.11N)$ is the Coulomb logarithm and the argument is appropriate for single-mass clusters (Giersz & Heggie 1994). To describe the fractional change of the cluster properties per τ_{rh} we define the following dimensionless parameters:

$$\epsilon \equiv -\frac{\dot{E}\tau_{\text{rh}}}{E}, \quad (4)$$

$$\lambda \equiv \frac{\dot{\kappa}\tau_{\text{rh}}}{\kappa}, \quad (5)$$

$$\mu \equiv \frac{\dot{r}_{\text{h}}\tau_{\text{rh}}}{r_{\text{h}}}, \quad (6)$$

$$\xi_{\text{e}} \equiv -\frac{\dot{N}\tau_{\text{rh}}}{N}. \quad (7)$$

In Gieles et al. (2011) it was assumed that the dimensionless rate of evolution of energy is constant during the entire evolution, i.e.

$$\epsilon = \zeta \simeq 0.1. \quad (8)$$

Here ζ can be interpreted as the efficiency of energy conduction of the cluster and depends on the stellar mass spectrum in the sense that clusters with a wider mass spectrum evolve faster (Spitzer & Hart 1971; Kim, Lee & Goodman 1998). In Paper I, we used $\epsilon = 0$ in the unbalanced phase (energy is conserved), which is accurate for isolated clusters and approximately correct for clusters in weak tidal fields. In this work, we allow for unbalanced evolution of the cluster such that $\epsilon \geq 0$ and $\epsilon \neq \zeta$ in the unbalanced phase (Section 2.3) and $\epsilon = \zeta$ in the balanced phase (Section 2.5). In the unbalanced phase, λ is positive because the cluster gets more concentrated and it is negative in the later evolution. In Paper I we considered clusters that start deeply embedded within r_{J} ($\mathcal{R}_{\text{h,J}} \equiv r_{\text{h}}/r_{\text{J}} \lesssim 1/30$), which means that μ is always positive in the initial phase of balanced evolution because the cluster expands to the tidal radius. In (roughly) the second half of the evolution μ is negative and equals approximately $-\xi_{\text{e}}/3$ because the cluster contracts at a (roughly) constant density in the tidal field (Hénon 1961; Gieles et al. 2011). In this paper we consider clusters that initially fill the Roche volume ($\mathcal{R}_{\text{h,J}} \simeq 0.1 - 0.2$) and for these clusters μ can be negative at the start of the evolution. The value of ξ_{e} is always positive, because \dot{N} is always negative.

If we multiply both sides of equation (2) by τ_{rh} we can write the evolution of the energy in terms of the dimensionless quantities defined in equations (4)-(7), i.e.

$$\epsilon = -\lambda + \mu + 2\xi_{\text{e}}. \quad (9)$$

The reader may have noted that we have not mentioned the core radius r_{c} so far, whilst we set out to include the evolution of r_{c} in the model. We have thus far omitted r_{c} from the equations because r_{c} only enters indirectly in the definition of E through κ , which can be interpreted as a concentration parameter. The concentration

of a cluster in the well-known King (1966) models is defined as the logarithm of the ratio $r_{\text{t}}/r_{\text{c}}$, where r_{t} is the King truncation radius which is the radius at which the density drops to zero. Here, we make the assumption that throughout the entire evolution κ depends only on the ratio $\mathcal{R}_{\text{ch}} \equiv r_{\text{c}}/r_{\text{h}}$, i.e. $\kappa = \kappa(\mathcal{R}_{\text{ch}})$, independent of the tidal truncation radius. This is motivated by the fact that the total energy is most sensitive to variations of the mass distribution within r_{h} , where the gravitational energy is highest. In Section 3, we show that results of N -body models support this assumption. To proceed, we introduce an additional dimensionless parameter

$$\delta \equiv \frac{\dot{r}_{\text{c}}\tau_{\text{rh}}}{r_{\text{c}}} \quad (10)$$

for the evolution of the core radius r_{c} on a τ_{rh} time-scale. To include δ in the energy equation (9) we take the time derivative of $\kappa(\mathcal{R}_{\text{ch}})$, using $\dot{\mathcal{R}}_{\text{ch}}/\mathcal{R}_{\text{ch}} = \dot{r}_{\text{c}}/r_{\text{c}} - \dot{r}_{\text{h}}/r_{\text{h}}$, such that

$$\frac{\dot{\kappa}}{\kappa} = \mathcal{K} \left(\frac{\dot{r}_{\text{c}}}{r_{\text{c}}} - \frac{\dot{r}_{\text{h}}}{r_{\text{h}}} \right), \quad (11)$$

with $\mathcal{K} \equiv \text{d} \ln \kappa / \text{d} \ln \mathcal{R}_{\text{ch}}$. With this expression we can relate the dimensionless parameter λ that describes the evolution of κ (equation 5) to the dimensionless parameters for the half-mass radius and core radius, μ (equation 6) and δ (equation 10), respectively,

$$\lambda = \mathcal{K}(\delta - \mu). \quad (12)$$

We substitute this in equation (9) to find

$$\epsilon = -\mathcal{K}\delta + (1 + \mathcal{K})\mu + 2\xi_{\text{e}}. \quad (13)$$

This equation relates the evolution of the total energy E to the evolution of the core radius r_{c} (through δ), the half-mass radius r_{h} (through μ) and the number of stars N (through ξ_{e}). It is this equation we are going to solve to get the time evolution of r_{c} , r_{h} and N in the unbalanced phase. Before we discuss the change of energy ϵ in the unbalanced phase in Section 2.3, we first discuss the rate at which the core radius contracts in the unbalanced phase.

2.2 Core contraction and gravothermal catastrophe

In the earliest phase of unbalanced evolution of a single-mass cluster the contracting core converts gravitational energy in kinetic energy which provides the energy that is required by two-body relaxation. Because the energy requirement is set by the cluster as a whole the core contracts on a half-mass relaxation time scale. Because of our definition of δ (equation 10) it follows that δ is approximately constant in that phase. When the relaxation time-scale of the core itself becomes much shorter than τ_{rh} then a runaway contraction follows. This process is often referred to as core collapse, or the gravothermal catastrophe (Lynden-Bell & Wood 1968) and it takes over from the slow contraction when the core radius becomes smaller than $r_{\text{c}} \lesssim 0.07r_{\text{h}}$ (Cohn 1980). From that moment the evolution of the core is decoupled from the evolution of the cluster and the core contracts self-similarly on a core relaxation time-scale τ_{rc} (Lynden-Bell & Eggleton 1980) until the collapse is halted by the formation of the first hard binary (in the absence of other energy sources, such as primordial binaries, a central black hole or stellar mass-loss, Heggie 1975). The definition of τ_{rc} is (Spitzer & Hart 1971)

$$\tau_{\text{rc}} = \frac{\sigma_{\text{c}}^3}{15.4G^2m\rho_{\text{c}} \ln(0.11N)}. \quad (14)$$

² The variation of the mean stellar mass as the result of mass-loss from stars and the preferential ejection of low-mass stars will be included in version 3 (Alexander et al. in preparation).

4 Gieles, Alexander, Lamers & Baumgardt

Here, σ_c^2 is the mean-square velocity of stars in the core and ρ_c is the core density. The core is to good approximation an isothermal system and σ_c^2 can be written as $\sigma_c^2 = (4/3)\pi G\rho_0 r_c^2$, where $\rho_0 \simeq 2\rho_c$ is the central density. During the gravothermal catastrophe the core density increases as

$$\rho_c = \rho_{c0} r_c^{-\alpha}, \quad (15)$$

where ρ_{c0} is a constant of proportionality and $2.2 \lesssim \alpha \lesssim 2.3$ (Lynden-Bell & Eggleton 1980; Heggie & Stevenson 1988; Baumgardt et al. 2003). For simplicity we assume that this relation holds during the entire unbalanced phase so we can write

$$\sigma_c^2 = \frac{8}{3}\pi G\rho_{c0} r_c^{2-\alpha}. \quad (16)$$

Now τ_{rc} is only a function of one variable (r_c) and two parameters (ρ_{c0} and α), which are determined in Section 3. For the rate of core contraction during the gravothermal catastrophe we use $\delta_2 = \dot{r}_c \tau_{rc} / r_c$. To ensure a smooth transition between the two different phases we define δ as

$$\delta = \delta_1 + \delta_2 \frac{\tau_{rh}}{\tau_{rc}}. \quad (17)$$

Here δ_1 is a negative constant that describes the speed of the initial contraction on a τ_{rh} time-scale and δ_2 is a negative constant that describes the gravothermal catastrophe on a τ_{rc} time-scale. For clusters that start with $r_c/r_h \gtrsim 0.07$ the second term on the right-hand side of equation (17) is initially small because $\tau_{rh}/\tau_{rc} \ll \delta_1/\delta_2$ and therefore $\delta \simeq \delta_1$. Whilst the core contracts at this rate, the ratio τ_{rh}/τ_{rc} grows and at some point the second term becomes dominant and during the runaway collapse we have $\delta \simeq \delta_2 \tau_{rh}/\tau_{rc}$. Combined with equation (10) we find that in this phase $\dot{r}_c/r_c = \delta_2/\tau_{rc}$. In Section 3 we will demonstrate that this simple linear addition of the two core contractions rates accurately describes the evolution of r_c and we determine the constants δ_1 and δ_2 from theory and N -body models.

Now that we have defined how δ depends on the other cluster parameters, we turn to the variation of ϵ in the unbalanced phase.

2.3 Unbalanced/pre-collapse evolution

To be able to numerically solve equation (13) we need to have an expression for the rate of change of energy ϵ in the unbalanced phase. In this phase the cluster has no energy source and the core contracts to generate heat. In isolation, the total energy of the cluster is conserved ($\epsilon = 0$, Paper I). In a tidal field, the energy of the cluster can change because of the escape of stars over the tidal boundary. This is an important effect to consider for clusters in a strong tidal field, because for these clusters more than half of the stars can escape before core collapse (e.g. Baumgardt 2001).

For most of the unbalanced phase the escape of stars happens on a relaxation time-scale because the outer parts of the cluster expand while the core contracts on a τ_{rh} time-scale (Section 2.2) and the response of the cluster can be implemented with straight forward energy considerations. Assume a cluster that has a large ratio $\mathcal{R}_{hJ} \simeq 0.1 - 0.2$, meaning that the cluster ‘fills’ the Roche volume. Then assume that stars gain energy by relaxation effects until they reach the escape energy and leave the cluster through the Lagrangian points with small velocities, such that the specific energy of the escaping stars is approximately $-GM/r_J$. The change in energy as a result of the loss of stars is thus $dE = -(GM/r_J)dM$.

Dividing this by E/τ_{rh} we find that the energy increase depends on the escape rate as

$$\epsilon = \frac{\mathcal{R}_{hJ}}{\kappa} \xi_e. \quad (18)$$

To understand the cluster’s response to the loss of stars, we substitute this expression for ϵ in equation (13) and find for the evolution of r_h

$$\mu = \frac{(\mathcal{R}_{hJ}/\kappa - 2) \xi_e + \mathcal{K}\delta}{1 + \mathcal{K}}. \quad (19)$$

Because τ_{rh} and all the terms on the right-hand side of equation (19) are functions of r_c , r_h , N and the angular frequency of the cluster about the Galaxy centre Ω , we can rewrite equation (19) as $\dot{r}_h(r_c, r_h, N, \Omega)$. This we can solve simultaneously with $\dot{r}_c(r_c, r_h, N)$ and $\dot{N}(r_c, r_h, N, \Omega)$ with a simple fourth order Runge-Kutta integrator, as in Paper I. To be able to solve these equations in time we need to have an expression for ξ_e , which is the topic of Section 2.6.

From equation (19) we see that the rate at which a cluster shrinks, or expands, depends critically on the ratio \mathcal{R}_{hJ} . Consider a Plummer model with $\mathcal{R}_{hJ} = 5\kappa/3$. Because for this model $\kappa \simeq 0.2$ we have $\mathcal{R}_{hJ} \simeq 0.333$ and we find that $\mu \simeq -(1/3)\xi_e$ (ignoring the small contribution of \mathcal{K}). This means that the half-mass radius shrinks as $N^{1/3}$ as the cluster loses stars. Because r_J also shrinks as $N^{1/3}$ in response to the escape of stars we find that for this \mathcal{R}_{hJ} the cluster shrinks at a constant density and, therefore, constant \mathcal{R}_{hJ} . For $\mathcal{R}_{hJ} \gtrsim 1/3$, and under the assumption that the density profile (i.e. κ) does not change, the cluster is unstable and will go into a runaway dissolution. For clusters with $\mathcal{R}_{hJ} < 5\kappa/3 \simeq 0.333$ r_h shrinks faster than r_J until an energy source becomes active.

Clusters in the post-collapse phase evolve roughly at a constant $\mathcal{R}_{hJ} \simeq 0.145$ (Hénon 1961), i.e. much lower than $1/3$. This is because the energy of these clusters changes not only because of a loss of stars over the tidal boundary, but also because of energy production in the core (see the discussion on p. 57 of Chapter 3.2 in Spitzer 1987). In the next Section we discuss the transition to the balanced phase.

2.4 Core collapse criterion and core evolution in the balanced phase

Before we can define the exact condition for the transition from unbalanced to balanced evolution it is necessary that we consider first the evolution of r_c in the balanced phase.

2.4.1 Core evolution in the balanced phase

In the balanced phase the size of r_c depends on the amount of energy that is produced, which in turn is set by the energy demand of the cluster as a whole (Hénon’s principle). For realistic clusters it can get complicated to understand this when we consider the combined effect of (primordial) binary stars, black holes, stellar mass-loss, etc. For single-mass clusters without primordial binary stars, however, it is possible to express the evolution of r_c in terms of r_h and N . With the assumption of energy balance and steady heating by binary stars that form in multiple encounters one can derive that in this phase the core radius depends on N and r_h as (see box 28.1 in Heggie & Hut 2003) $r_c = (N/N_2)^{-2/3} r_h$, where N_2 is a constant that will be determined in Section 3. The evolution of r_c

is passive, in the sense that it follows the evolution of N and r_h which follow from the assumption of balanced evolution (Gieles et al. 2011; Paper I).

For clusters with $N \gtrsim 7000$ there is no steady core evolution, but the core undergoes gravothermal oscillations (Bettwieser & Sugimoto 1984; Goodman 1987). We do not include these oscillations of the core, although a simple prescription exists (Allen & Heggie 1992). Instead, we assume that for large N the ratio \mathcal{R}_{ch} tends to a constant $\mathcal{R}_{\text{ch}} \simeq (N_3/N_2)^{-2/3}$, where $N_3 \simeq 7000$ is the boundary between clusters for which \mathcal{R}_{ch} evolves as $N^{-2/3}$ (i.e. for $N \lesssim N_3$) and those for which \mathcal{R}_{ch} is constant (i.e. for $N \gtrsim N_3$). The exact value for N_3 will be determined in Section 3. To implement the convergence to a constant \mathcal{R}_{ch} for clusters with large N we use

$$\mathcal{R}_{\text{ch}} = \left(\frac{N_2}{N} + \frac{N_2}{N_3} \right)^{2/3}, \quad (20)$$

$$\simeq \begin{cases} (N/N_2)^{-2/3} & \text{for } N \ll N_3; \\ (N_3/N_2)^{-2/3} & \text{for } N \gg N_3. \end{cases} \quad (21)$$

Taking the time derivative of equation (20) and multiplying by τ_{rh} we find an expression for δ in the post-collapse phase

$$\delta = \frac{2}{3} \xi_e \left(1 + \frac{N}{N_3} \right)^{-1} + \mu. \quad (22)$$

For large $N \gg N_3$ the core radius evolves at the same rate as the half-mass radius because the first term on the right-hand side is negligible and therefore $\delta \simeq \mu$, while for $N \lesssim N_3$ the ratio \mathcal{R}_{ch} grows as $N^{-2/3}$ while N decreases. The evolution of r_h (i.e. μ) is discussed in Section 2.5.

For the evolution of the core density ρ_c we assume that between r_c and r_h the cluster is approximately isothermal and has a density distribution $\rho \propto r^{-2}$, such that

$$\rho_c = \rho_h \mathcal{R}_{\text{ch}}^{-2}, \quad (23)$$

where $\rho_h = 3M/(8\pi r_h^3)$ is the average density within r_h .

Now we have defined the equilibrium evolution of r_c and \mathcal{R}_{ch} in the balanced phase, we consider the transition from unbalanced to balanced evolution.

2.4.2 Criterion for core collapse

We define the moment of core collapse as the moment in the evolution that \mathcal{R}_{ch} has reached the value of the relation for \mathcal{R}_{ch} as a function of N in the balanced phase (equation 20). At each time step in the unbalanced phase the criterion changes because it depends on the instantaneous value of \mathcal{R}_{ch} and N . This allows us to make the transition to the balanced evolution without a priori (i.e. before the evolution starts) knowledge of the exact *moment* of core collapse. Core collapse time is well understood for isolated, single-mass, Plummer models: roughly 17 initial τ_{rh} (e.g. Larson 1970; Aarseth, Henon & Wielen 1974), but it is hard to predict what it is when the cluster loses a significant number of stars in the unbalanced phase, or starts with a smaller core. Both effects are now included in the EMACSS model. The way we make the transitions causes us to underestimate the maximum core density in the collapse. This is because after core collapse the core expands towards larger radii and this core bounce (Inagaki & Lynden-Bell 1983) is not included in the model. This effect can be seen in the N -body

models (see Section 3). The relation we propose describes the evolution of r_c near the maxima after core bounce and is therefore a reasonable description for the majority of the evolution.

2.5 Half-mass radius in balanced evolution

Combining equation (22) with the relation for the total energy variation (equation 13) we find that the half-mass radius evolution in balanced evolution relates to ζ and ξ_e as

$$\mu = \zeta + \left(\frac{2}{3} \mathcal{K} \left[1 + \frac{N}{N_3} \right]^{-1} - 2 \right) \xi_e. \quad (24)$$

If we ignore the variation of the density profile due to the evolution of r_c (i.e. $\mathcal{K} = 0$) we find $\mu = \zeta - 2\xi_e$, i.e. the relation that was used in Paper I. The small \mathcal{K} dependent term in equation (24) is the only difference with the radius evolution in the balanced phase presented in Paper I. The consequence of this difference is that the evolution of r_h and r_v is slightly different in the balanced phase for clusters with $N \lesssim N_3$, whereas in Paper I we assumed $r_h/r_v = 1$. In the next section, we discuss the escape rate ξ_e in both the unbalanced and the balanced evolution.

2.6 Escape rate

Up to this point, we have expressed the evolution in terms of N and the dimensionless escape rate ξ_e . To be able to solve all relations in time, we need an expression for ξ_e and the initial number of stars N . In this section, we find expressions for ξ_e in the balanced phase (Section 2.6.1) and in the unbalanced phase (Section 2.6.2). From the N -body simulations (Section 3), we find that ξ_e in the unbalanced phase is lower than what we found for the balanced evolution in Paper I. An increase of the mass-loss rate after core collapse was also found for multimass model by Lamers, Baumgardt & Gieles (2010). Before we can describe ξ_e in the unbalanced phase, we need to first recall the definition of ξ_e in the balanced phase as described in detail in Paper I.

2.6.1 Escape rate in the balanced phase

In this section, we discuss the escape rate of stars in the balanced phase by recalling the framework described in Paper I. The arguments used in Paper I follow from the results of Gieles & Baumgardt (2008), who find that the escape rate in N -body models of tidally limited clusters depends on the ratio $\mathcal{R}_{h,j}$ and N as $\xi_e \propto \mathcal{R}_{h,j}^{3/2} N^{1/4}$. The scaling $\mathcal{R}_{h,j}^{3/2}$ is because the escape energy is lower for larger $\mathcal{R}_{h,j}$, which makes it easier for a larger fraction of the stars to escape in a τ_{rh} time-scale. The scaling with $N^{1/4}$ is because of the delayed escape of stars from the anisotropic Jacobi surface (Fukushige & Heggie 2000), which preferentially slows down the escape of stars from low- N systems (Baumgardt 2001). Isolated clusters lose a small fraction (approximately a percent) of their stars every relaxation time (Baumgardt et al. 2002). To include both effects, we used the following expression for ξ_e in Paper I

$$\xi_e = \xi_{e1}(1 - \mathcal{P}) + \frac{3}{5} \zeta \mathcal{P}, \quad (25)$$

where $\xi_{e1} = 0.0142$ (Paper I) is the escape rate for isolated clusters and

$$\mathcal{P} = \left(\frac{\mathcal{R}_{vJ}}{\mathcal{R}_{vJ1}} \right)^z \left(\frac{N \log[0.11N_1]}{N_1 \log[0.11N]} \right)^{1-x}, \quad (26)$$

with $z = 1.61$ (Paper I), $x = 0.75$ (Baumgardt 2001; Paper I) and $\mathcal{R}_{vJ1} = 0.145$ (Hénon 1961; Paper I). In weak tidal fields $\mathcal{P} \simeq 0$ and $\xi_e \simeq \xi_{e1}$, a constant rate of escape per relaxation time, while for tidally limited clusters the quantity $\mathcal{P} \simeq 1$ and $\xi_e \simeq (3/5)\zeta \simeq 0.06$. The scaling constant N_1 was determined in Paper I ($N_1 = 38\,252$), but in Section 3 we slightly revise this value. This is because in equation (26) we use r_v in the ratio \mathcal{R}_{vJ} and τ_{rh} is expressed in terms of r_h , and in the current version r_h/r_v is allowed to evolve, whereas in Paper I r_h was always equal to r_v .

2.6.2 Escape rate in the unbalanced phase

The expression for ξ_e in the unbalanced phase should satisfy three conditions: first, isolated clusters lose almost no stars (Baumgardt et al. 2002); secondly, the escape rate of Roche volume filling clusters is about $f \simeq 0.3$ times that in the balanced phase and, finally, it should connect to ξ_e in the balanced phase. We therefore adopt the following relation for ξ_e in the unbalanced phase

$$\begin{aligned} \xi_e &= \mathcal{F}\xi_{e1}(1 - \mathcal{P}) + (f + [1 - f]\mathcal{F})\frac{3}{5}\zeta\mathcal{P}, \quad (27) \\ &= \begin{cases} f(3/5)\zeta\mathcal{P} & \text{for } \mathcal{F} = 0; \\ \xi_{e1}(1 - \mathcal{P}) + (3/5)\zeta\mathcal{P} & \text{for } \mathcal{F} = 1. \end{cases} \quad (28) \end{aligned}$$

Here $\mathcal{F} = \mathcal{R}_{ch}^{\min}/\mathcal{R}_{ch}$ and \mathcal{R}_{ch}^{\min} is the minimum ratio of $\mathcal{R}_{ch}(N)$ in the unbalanced phase and is reached at the moment of core collapse (equation 20). In the beginning of the evolution of low-concentration clusters (such as Plummer models), we have $\mathcal{R}_{ch} \gg \mathcal{R}_{ch}^{\min}$ and therefore $\mathcal{F} \simeq 0$ and there is only a contribution from escapers due to the tidal truncation: $\xi_e \simeq f(3/5)\zeta$. This relation ensures that $\xi_e \simeq 0$ for isolated clusters in the unbalanced phase, as it should. Close to core collapse $\mathcal{R}_{ch} \simeq \mathcal{R}_{ch}^{\min}$ and therefore $\mathcal{F} \simeq 1$ such that both the term due to escapers in isolation and the term due to escapers in the tidal field approach the values in balanced evolution.

In the next section we discuss the implementation of these equations in EMACSS and a comparison to N -body simulations.

3 IMPLEMENTATION AND COMPARISON TO N -BODY SIMULATIONS

3.1 Description of N -body simulations

Here we describe the details of a suite of direct N -body simulations to benchmark the EMACSS model against. We model clusters with five different values of N ranging from $N = 4\,096$ to $65\,536$ with steps of a factor of two. All stars have the same mass and the clusters were initially described by Plummer (1911) models or King (1966) models with $W_0 = 5$ with isotropic velocity distributions. The latter model was used for the simulations of clusters in strong tidal fields to avoid having stars above the escape energy. We used the standard N -body units, such that $G = M = -4E = 1$ (Heggie & Mathieu 1986). The virial radius r_v is defined as $r_v = -GM^2/(2W)$, where W is the gravitational energy. We assume that the clusters are in virial equilibrium initially, such that $W = 2E$ and $r_v = 1$. In this case, the conversion factor for time in physical units (t^*) relates to the value of r_v in physical units (r_v^*)

and the mass in physical units (M^*) as $t^* = (GM^*/r_v^{*3})^{-1/2}$. The half-mass radii for the Plummer and King models in these units are $r_h \simeq 0.78$ and 0.82 respectively. The initial value for κ for the two models is thus $\kappa_0 \simeq 0.195$ and 0.205 . In EMACSS κ_0 is computed from the initial r_h as $\kappa_0 = r_h/4$ (because $r_v = 1$).

The equation of motion of the stars was solved in a reference frame that corotates with the circular orbit of the cluster about a point-mass galaxy. The centrifugal, Coriolis and tidal forces were added to the forces due to the other $N - 1$ stars (equation 1 in Giersz & Heggie 1997). The strength of the tidal field can be quantified by the angular frequency Ω of the cluster orbit. For a circular orbit around a point-mass galaxy the Jacobi radius r_J of the cluster depends on Ω and the mass of the cluster M as

$$r_J = \left(\frac{GM}{3\Omega^2} \right)^{1/3}. \quad (29)$$

We modelled four sets of clusters with different initial ratios \mathcal{R}_{hJ} . Two sets of compact (in terms of \mathcal{R}_{hJ}) clusters were presented in Paper I. These clusters were initially described by Plummer models and the two sets had initial values of $\mathcal{R}_{hJ} = 1/100$ and $1/30$. For this study we ran two additional sets of ‘Roche filling’ clusters with $\mathcal{R}_{hJ} = 1/10$ (Plummer) and a series of King (1966) models with $W_0 = 5$. For the latter set of runs $\mathcal{R}_{hJ} = 1/5.37$, but we will refer to these runs as $\mathcal{R}_{hJ} = 1/5$. For low- N clusters multiple simulations were done to average out statistical fluctuations, in the same way as was done in Paper I: for $N = [4\,096, 8\,192, 16\,384, 32\,768, 65\,536]$ we ran $[16, 8, 4, 2, 1]$ simulations, respectively.

Stars are counted as members when their distance to the centre of the cluster is less than r_J and stars are removed from the simulation if their distance from the cluster centre exceeds $2r_J$. The Jacobi radius r_J and the number of members are calculated iteratively using equation (29). The core radius is defined as in chapter 15.2 of Aarseth (2003) and with this definition for r_c both the Plummer model and the King model with $W_0 = 5$ have $\mathcal{R}_{ch} \simeq 0.4$. The energy E of the cluster is defined as the external energy (kinetic and potential components of single stars and the centres of mass of multiples, see Giersz & Heggie 1997) separately from the internal energy of particles (i.e. the energy stored in binaries and multiples). For all simulations we used the N -body code NBODY6, which is a fourth order Hermite integrator with Ahmad & Cohen (1973) neighbour scheme (Makino & Aarseth 1992; Aarseth 1999, 2003) with accelerated force calculation on NVIDIA Graphics Processing Units (Nitadori & Aarseth 2012). In the next sections, we compare the results of the N -body models to EMACSS and determine the parameters. To do this, we isolate the various physical process and build up the model piece by piece in Sections 3.2 to 3.4 to find the values of the parameters of the various physical processes described in Section 2. The fluctuations that occur in small N systems are taken into account by comparing EMACSS to the average of the results for the individual runs with the same initial condition, but different random seeds. The final best-fitting parameters of EMACSS are summarized in Table 1.

3.2 Relation between κ and \mathcal{R}_{ch}

The first thing we determine from the N -body simulations is the relation between κ and the ratio \mathcal{R}_{ch} (Section 2.1). The points were computed as follows: for 20 runs with N ranging from $N = 4\,096$ to $65\,536$ with steps of 2, and $\mathcal{R}_{hJ} = 1/5, 1/10, 1/30$ and $1/100$ we determined the values of κ and $\log \mathcal{R}_{ch}$ from the individual

simulations. All runs follow similar tracks, but the relation $\kappa(\mathcal{R}_{\text{ch}})$ in the unbalanced phase is different from the relation in the balanced phase. In the balanced phase, there is an indication that κ is smaller for larger N models at low values of \mathcal{R}_{ch} , but we will not include this small N dependence in the model. The difference between the unbalanced and balanced curves is most likely due to the difference in density profile: in the unbalanced phase the cluster starts with a large core and during the collapse it develops an $r^{-2.2}$ cusp in the central density profile. In the balanced phase, the central density profile is almost isothermal and the central density cusp is r^{-2} . Because of this difference, we describe the $\kappa(\mathcal{R}_{\text{ch}})$ relation in the different phases with different functions. To separate the evolution in the two phases we have to find a definition of core collapse in these models. We define core collapse as the moment when the total energy E increases by more than 5% in a unit of N -body time. Such a sharp increase in E is not found at any other moment in all runs and turns out to be a useful definition for all simulations. For both the balanced and the unbalanced phase, the median of κ was found in 50 bins that were equally spaced in $\log \mathcal{R}_{\text{ch}}$. A minimum of $N = 200$ remaining stars was used. In Fig. 1, we show the κ values of the N -body models as dots with the results for the unbalanced and the balanced phase in the top and bottom panels, respectively.

We find that for both evolutionary phases the κ values can be well described by an error function of the form

$$\kappa(\mathcal{R}_{\text{ch}}) = \kappa_1 + (\kappa_0 - \kappa_1) \operatorname{erf} \left(\frac{\mathcal{R}_{\text{ch}}}{\mathcal{R}_{\text{ch}0}} \right). \quad (30)$$

The values for the constants are given in Table 1 and we note that for the unbalanced phase $\kappa_0 = r_{\text{h}}/(4r_{\text{v}})$ depends on the initial density profile of the cluster. For this function the logarithmic derivative \mathcal{K} (equations 11 & 12) is

$$\mathcal{K} = \frac{\mathcal{R}_{\text{ch}}}{\kappa} \frac{2(\kappa_0 - \kappa_1) \exp(-\mathcal{R}_{\text{ch}}^2/\mathcal{R}_{\text{ch}0}^2)}{\sqrt{\pi} \mathcal{R}_{\text{ch}0}} \quad (31)$$

and for the parameters used here we find $-0.1 \lesssim \mathcal{K} < 0$.

The last point of consideration is the connection between $\kappa(\mathcal{R}_{\text{ch}})$ in the unbalanced phase and $\kappa(\mathcal{R}_{\text{ch}})$ in the balanced phase. Because the constant κ_1 is different in these two phases the function $\kappa(t)$ is discontinuous at core collapse if we simply jump to the new $\kappa(\mathcal{R}_{\text{ch}})$ relation at core collapse. This would also result in a discontinuity in the energy evolution, which is not desirable. We therefore add a term to λ in the balanced phase that ensures that $\kappa(t)$ is continuous and that κ evolves to the relation $\kappa(\mathcal{R}_{\text{ch}})$ of equation (30) with the parameters appropriate for the balanced phase on a τ_{th} time-scale. The functional form for λ we use in the balanced phase is

$$\lambda = \mathcal{K}(\delta - \mu) + \frac{\kappa(\mathcal{R}_{\text{ch}}) - \kappa}{\kappa(\mathcal{R}_{\text{ch}})}. \quad (32)$$

At the start of balanced evolution (i.e. at core collapse) κ is higher than $\kappa(\mathcal{R}_{\text{ch}})$, such that the added term on the right-hand side of equation (32) is negative. The difference between κ and $\kappa(\mathcal{R}_{\text{ch}})$ gets smaller every integration step and κ approaches $\kappa(\mathcal{R}_{\text{ch}})$ asymptotically. We do not include this extra term in the energy balance (equation 19) such that the system is slightly out of balance, in the sense that $\epsilon \gtrsim \zeta$, for a fraction of a relaxation time after core collapse. This phase can be interpreted as the ‘core bounce’ phase (Inagaki & Lynden-Bell 1983) in which excess energy is released

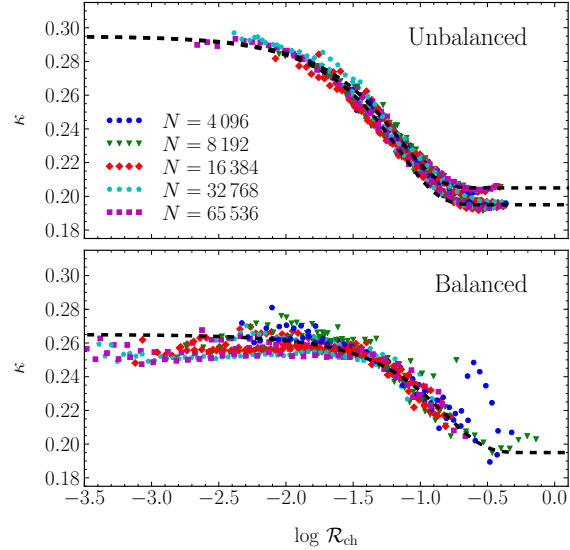


Figure 1. The evolution of κ as a function of the ratio $\mathcal{R}_{\text{ch}} = r_c/r_h$ for clusters in the unbalanced (pre-collapse) phase (top) and in the balanced (post-collapse) phase (bottom). The dashed lines approximate the N -body results with error functions (equation 30). In the unbalanced phase there are two dashed lines shown: the top line corresponds to the King (1966) models ($\kappa_0 \simeq 0.205$) and the bottom line corresponds to the Plummer (1911) models ($\kappa_0 \simeq 0.195$).

by the newly formed binary star(s) which is diffused by two-body relaxation.

The \mathcal{K} values are quite low and \mathcal{K} , therefore, affects the evolution only mildly. In Paper I, we ignored the variation of κ and we assumed that $r_{\text{h}} = r_{\text{v}}$ throughout the evolution. For the N -body models, initially $r_{\text{h}} \simeq 0.8r_{\text{v}}$ and the evolution of κ in the unbalanced phase causes the ratio $r_{\text{h}}/r_{\text{v}}$ to grow to approximately unity (Section 3.3). If N becomes smaller than a few thousand the cluster evolves to low concentration again.

3.3 Evolution of the core parameters

To quantify the rate of core contraction we first consider the evolution of the core parameters that define the core relaxation time-scale τ_{rc} (equation 14). In Fig. 2, we show the average density within the core ρ_c as a function of r_c in the unbalanced phase for clusters with various initial N . The average core density ρ_c is defined as $3M_c/(4\pi r_c^3)$, where M_c is the total mass of the stars in the core. At the start of the evolution all models start with $\rho_c \simeq 0.7$ and $r_c \simeq 0.3$. When r_c shrinks the density increases as

$$\rho_c = 0.055 r_c^{-2.2}, \quad (33)$$

which corresponds to the dashed line in Fig. 2. This value of $\alpha = 2.2$ is close to what was found in previous studies. Lynden-Bell & Eggleton (1980) used theoretical arguments for the self-similar evolution of the core near the gravothermal catastrophe and found $\alpha = 2.21$. Heggie & Stevenson (1988) found a logarithmic slope of -2.23 from Fokker-Planck models of the late stages of core collapse and Baumgardt et al. (2003) found a value of -2.26 from N -body models of single-mass clusters. We note that our slightly smaller value of -2.2 is probably because we use this relation to

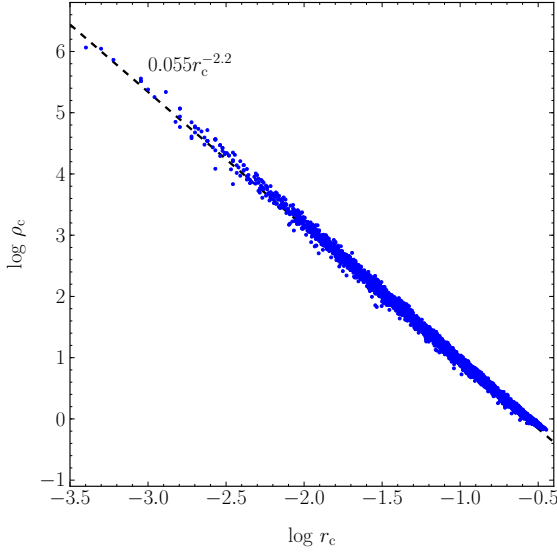


Figure 2. Relation between core (mass) density ρ_c and core radius r_c in the unbalanced phase for N -body models for the $\mathcal{R}_{h,J} = 1/5$ models and the $\mathcal{R}_{h,J} = 1/100$ models. For each of the $\mathcal{R}_{h,J}$ sets a model for each N is shown. The tight correlation in the N -body data justifies a single relation for $\rho_c(r_c)$ for all models. The line shows the relation of equation (33).

describe the entire core contraction phase starting at $t = 0$, while the studies mentioned above determined α in the final stages of core contraction (the gravothermal catastrophe). With equation (33) and the expression for the central velocity dispersion σ_c (equation 16) we have all parameters of the core defined to be able to define τ_{rc} (equation 14).

Now we have defined how ρ_c depends on r_c we can turn to the evolution of r_c . Fig. 3 shows the evolution of N , r_h and r_c as a function of time following from N -body models, expressed in the initial τ_{rh} , for clusters with different N and $\mathcal{R}_{h,J}$. In the left-hand panels, the results for clusters with $N = 4096$ are shown and in the right-hand panels, we show the results for $N = 65536$. Each panel contains results for clusters with $\mathcal{R}_{h,J} = 1/5$ and $1/100$. The data points were selected to be in the unbalanced phase (pre-collapse) in the same way as described in Section 3.2.

Initially, the core radius shrinks exponentially (i.e. a straight line in logarithmic-linear plot), which is because of the contraction on a τ_{rh} time-scale. We find that $\delta_1 \simeq -0.09$ (see equation 17) describes the initial core contraction of the N -body models very well. For the clusters with $\mathcal{R}_{h,J} = 1/100$ the core radius evolution accelerates after about 15 initial τ_{rh} and r_c contracts on a τ_{rc} time-scale. This happens earlier for the $\mathcal{R}_{h,J} = 1/5$ clusters because τ_{rh} shrinks because of the escaping stars (top panels) and the shrinking r_h (middle panels).

For the rate of runaway collapse (δ_2), we find that a value of $\delta_2 = 0.002$ provides a good description. From Fokker-Planck models Cohn (1980) finds that in this phase the core density increases at a rate $\dot{\rho}_c \tau_{rc} / \rho_c \simeq 0.0036$ and Baumgardt et al. (2003) find $\dot{\rho}_c \tau_{rc} / \rho_c \simeq 0.003$ from N -body models. Because of the self-similar nature of the collapse ($\rho_c \propto r_c^{-\alpha}$) we can relate this parameter to δ_2 (equation 17) as $\delta_2 = -\alpha^{-1} \dot{\rho}_c \tau_{rc} / \rho_c$ (see equation 17, such that the results of Cohn (1980) and Baumgardt et al. (2003) translate into $\delta_2 \simeq 0.0016$ and $\delta_2 \simeq 0.0014$, respectively. It is not a concern that we need a slightly larger value for δ_2 to get a

good description of r_c , because EMACSS does not evolve r_c to the same small values as the Fokker-Planck and N -body models, because we switch to balanced evolution once \mathcal{R}_{ch} reaches the value of balanced evolution (Section 2.4).

The middle panels of Fig. 3 show the evolution of r_h . For the clusters with $\mathcal{R}_{h,J} = 1/100$ the increase of r_h from $r_h \simeq 0.78$ initially to $r_h \simeq 1$ at core collapse is due to the changing density profile which was already seen in the increase of κ (Fig. 1). When escaping stars can be ignored the rate of increase of r_h relates to the rate of change of r_c as $\mu = \mathcal{K}\delta/(1+\mathcal{K})$ (equation 13). This relation nicely describes both the evolution of r_c and r_h , also in the presence of escapers as can be seen for the models with $\mathcal{R}_{h,J} = 1/5$. We find that EMACSS slightly underestimates the moment of core collapse for the $\mathcal{R}_{h,J} = 1/5$ models and EMACSS overestimates this moment for the $\mathcal{R}_{h,J} = 1/100$ models. The differences in core collapse times are in all cases less than approximately 6%.

The top panels of Fig. 3 show that the clusters in strong tidal fields ($\mathcal{R}_{h,J} = 1/5$) lose more than half their stars before core collapse. The escape rate ξ_e in this phase is discussed in more detail in the next section.

3.4 Escape rate

In Fig. 4, we show the dimensionless escape rate ξ_e as a function of $\mathcal{R}_{v,J}$ for the entire evolution of clusters with different N ($N = 4096$ and 65536) for the four different initial $\mathcal{R}_{h,J}$. The dependence of ξ_e on N and $\mathcal{R}_{v,J}$ is well described by equation (27) and an escape rate due to the tides in the unbalanced phase that is three times lower than what it is in the balanced phase (i.e. $f = 0.33$). When the clusters reach the balanced phase the ξ_e curves turn by about 90° and the subsequent evolution and corresponding N and $\mathcal{R}_{v,J}$ dependence is well described by the relation from Paper I (equations 25 and 26).

3.5 Integration steps

In Paper I, we adopted an integration step of $\Delta t = 0.1\tau_{rh}$. Here, we need to take smaller steps in the unbalanced phase when the core shrinks on a τ_{rc} time-scale. We therefore use in the unbalanced phase

$$\Delta t = [(100\tau_{rc})^{-1} + (0.1\tau_{rh})^{-1}]^{-1}. \quad (34)$$

For small τ_{rc} near core collapse the step size is $\Delta t \simeq 100\tau_{rc}$. A step size of $100\tau_{rc}$ is justified by the fact that the core parameters vary only by a fraction of a per cent near core collapse (Section 3.3) and with this step size we therefore still under-sample the evolution of the core. A convergence test showed that the final results change by less than 1% if we decrease Δt by a factor of 100. In the balanced phase we use $\Delta t = 0.1\tau_{rh}$, as in Paper I. EMACSS outputs the data every $0.1\tau_{rh}$.

4 GENERAL RESULTS

In Figs 5 and 6 we show the results of the evolution of all parameters for the N -body runs with initial $\mathcal{R}_{h,J} = 1/5$ and $1/10$, respectively. The results following from EMACSS are shown as dashed lines and provide an accurate description of r_c , r_h , r_J (i.e. N). The evolution of the derived quantities ρ_c , E and κ are also well reproduced. If we consider the temporal aspects of evolution, such as

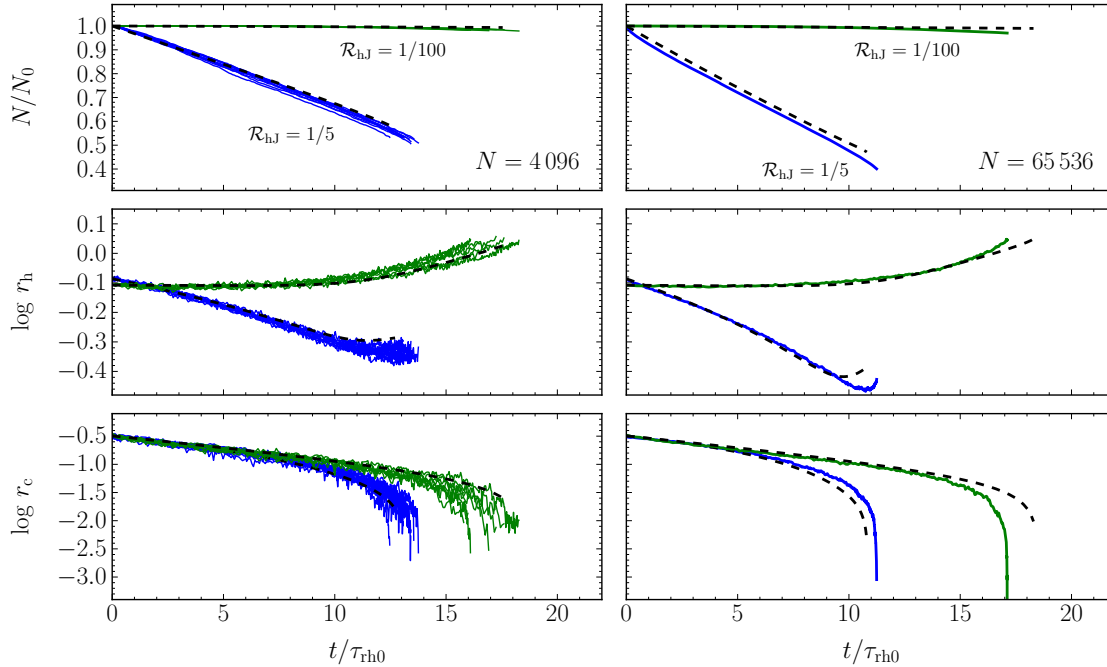


Figure 3. Evolution of N (top row), the half-mass radius r_h (middle row) and the core radius r_c (bottom row) in the unbalanced phase for clusters with different initial N : the 16 different realizations of the $N = 4096$ model are shown in the left-hand panels and the $N = 65536$ models are shown in the right-hand panels. Each panel shows the results for $\mathcal{R}_{hJ} = 1/5$ (blue, bottom) and $\mathcal{R}_{hJ} = 1/100$ (green, top). The dashed lines show the result of EMACSS based on the expressions for the evolution of r_c (δ , equation 10) and r_h (μ , equation 19).

Table 1. Summary of all the parameters in EMACSS

Process	Quantity	Unbalanced	Balanced	Equation
Energy diffusion	ζ	0.1	0.1 [†]	(8)
r_c evolution	δ_1	-0.09^{\ddagger}		(10,17)
	δ_2	-0.002^{\ddagger}		(10,17)
	ρ_{c0}	0.055		(15)
	α	2.2		(15)
Concentration	\mathcal{R}_{ch0}	0.100	0.220	(30)
	κ_0	$r_h/(4r_v)$	0.200	(30)
	κ_1	0.295	0.265	(30)
Escape rate ξ_e	f	0.3		(27)
	ξ_{e1}	0.0142	0.0142*	(25,27)
	x	0.75	0.75*	(26)
	z	1.61	1.61*	(26)
	\mathcal{R}_{vJ1}	0.145	0.145*	(26)
\mathcal{R}_{ch} evolution	N_1	15000	15000 [†]	(26)
	N_2		12	(20)
	N_3		15000 [†]	(20)

Notes: [†] the values found in Paper I are slightly adjusted; [‡] in the code these values are normalised to ζ , such that the user can choose to use a different value of ζ and adjust the speed of the entire evolution; * from Paper I.

the moment of core collapse and the total lifetime then the difference between the EMACSS results and the N -body results is within approximately 10% for these models.

Figs 7 and 8 show the results for the compact clusters of Paper I with initial $\mathcal{R}_{hJ} = 1/30$ and $\mathcal{R}_{hJ} = 1/100$, respectively. For these clusters, the evolution of EMACSS is very similar to the version presented in Paper I and the good agreement between

EMACSS and the N -body models is therefore as expected. A small difference with Paper I is that we here compare the model to the half-mass radius r_h and the virial radius r_v (through κ), whereas in Paper I we only considered the virial radius because we assumed $r_h = r_v$.

The only parameters we have not discussed yet are N_2 and N_3 (equation 20). From a comparison of EMACSS to the asymptotic evolution of $\mathcal{R}_{ch}(N)$ we find $N_2 = 12$. The model is not very sensitive to the exact value of N_3 . Clusters with $N \gtrsim N_3$ evolve at constant \mathcal{R}_{ch} in the balanced phase, whereas clusters with $N \lesssim N_3$ evolve as $\mathcal{R}_{ch} \propto N^{-2/3}$ (Section 2.4.1). We find that for a value of $N_3 = N_1 = 15000$ EMACSS provides a satisfactory description of r_c for all runs. A summary of all model parameters is given in Table 1.

5 CONCLUSIONS AND FUTURE WORK

The new version of EMACSS reproduces the evolution of the three fundamental radii of single-mass clusters evolving in a steady tidal field: the core radius r_c , the half-mass radius r_h and the Jacobi (or tidal) radius r_J , where the latter is equivalent to the evolution of the total mass M , or the number of stars N . Compared to version one (Paper I) the code now also reproduces the unbalanced evolution which is important for clusters in strong tidal fields (i.e. large initial \mathcal{R}_{hJ}). This version also introduces the evolution of the core density ρ_c and a related cluster concentration parameter $\kappa = r_h/(4r_v)$ that depends on the ratio $\mathcal{R}_{ch} = r_c/r_h$. The evolution of the core parameters introduces an additional number of integrations steps compared to Paper I, most of which are in the phase just before core collapse (the gravothermal catastrophe), when the core contracts

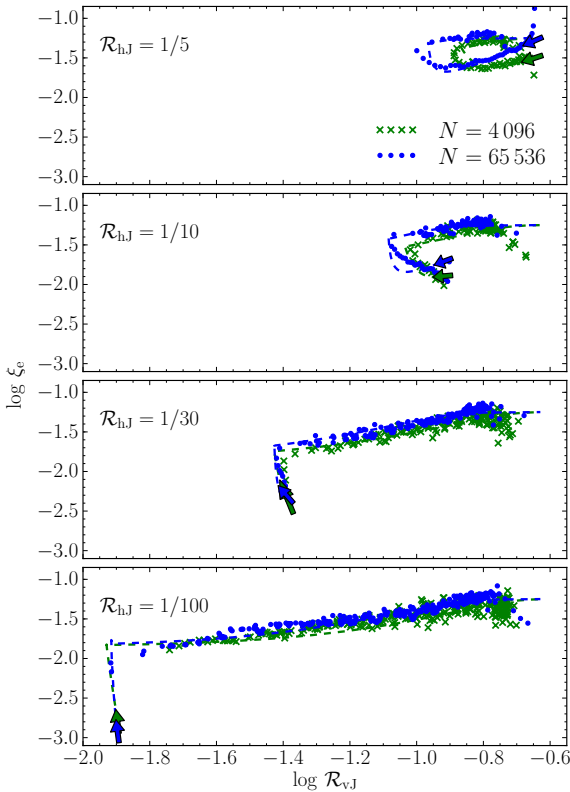


Figure 4. Dimensionless escape rate ξ_e for clusters with $N = 4096$ (green crosses) and $N = 65536$ (blue dots) for different initial $\mathcal{R}_{h,J}$. The derivative \dot{N} for the N -body data was found numerically from the average $N(t)$ data by dividing the evolution of N in approximately 100 equal steps ΔN which were divided by the corresponding steps Δt . The start and the direction of the evolution of the EMACSS result is indicated with an arrow. The dashed lines are the results from EMACSS using equation (27) for the unbalanced phase which connects to the relation for the balanced phase of Paper I (equation 25). Clusters in a strong tidal field (two top panels) initially contract, i.e. the ratio $\mathcal{R}_{v,J}$ becomes smaller and the cluster moves to the left in this figure. Clusters in weak tidal fields (bottom two panels) lose very few stars in the unbalanced phase. Towards core collapse ξ_e increases until it reaches the balanced track (Paper I and equation 25) where the ξ_e curves show a sharp bend of approximately 90° .

on a core relaxation time. Still, the entire evolution is solved with a modest number of about 2000 integration steps, such that about 10^3 models can be computed in a second on a single-core desktop computer.

In a follow-up paper (Alexander et al., in preparation, Paper III), we expand EMACSS to reproduce clusters with more realistic (initial) properties such as a stellar mass function, and the evolution and mass-loss of stars. Both code modules (single-mass and multi-mass) will be available in the same code and a command line switch allows the user to select one of them. It is worth noting that the computational effort for solving cluster evolution is almost N -independent, which makes EMACSS a powerful tool to do population synthesis studies of globular cluster populations (Alexander & Gieles 2013; Alexander et al., in preparation).

ACKNOWLEDGEMENT

PA acknowledges STFC for financial support. MG acknowledges financial support from the Royal Society in the form of a University Research Fellowship (URF) and an equipment grant that was used to purchase nodes equipped with Graphics Processing Units (GPUs) that were used for the N -body computations. All authors thank the Royal Society for an International Exchange Grant between the UK and the University of Queensland in Brisbane. HB is supported by the Australian Research Council through Future Fellowship grant FT0991052. All authors thank Sverre Aarseth for his support of NBODY6 and Keigo Nitadori for the GPU implementation. Douglas Heggie is acknowledged for several interesting discussions and for constructive comments on the manuscript. The authors thank the referee Mirek Giersz for carefully reading the paper and for providing constructive comments.

REFERENCES

- Aarseth S. J., 1999, *PASP*, 111, 1333
Aarseth S. J., 2003, *Gravitational N-Body Simulations*. Cambridge University Press
Aarseth S. J., Heggie D. C., 1998, *MNRAS*, 297, 794
Aarseth S. J., Hénon M., Wielen R., 1974, *A&A*, 37, 183
Ahmad A., Cohen L., 1973, *J. of Comput. Phys.*, 12, 389
Alexander P. E. R., Gieles M., 2012, *MNRAS*, 422, 3415 (Paper I)
Alexander P. E. R., Gieles M., 2013, *MNRAS*, 432, L1
Allen F. S., Heggie D. C., 1992, *MNRAS*, 257, 245
Baumgardt H., 2001, *MNRAS*, 325, 1323
Baumgardt H., Heggie D. C., Hut P., Makino J., 2003, *MNRAS*, 341, 247
Baumgardt H., Hut P., Heggie D. C., 2002, *MNRAS*, 336, 1069
Bettwieser E., Sugimoto D., 1984, *MNRAS*, 208, 493
Brodie J. P., Strader J., 2006, *ARA&A*, 44, 193
Cohn H., 1980, *ApJ*, 242, 765
Eldridge J. J., Izzard R. G., Tout C. A., 2008, *MNRAS*, 384, 1109
Freeman K., Bland-Hawthorn J., 2002, *ARA&A*, 40, 487
Fukushige T., Heggie D. C., 1995, *MNRAS*, 276, 206
Fukushige T., Heggie D. C., 2000, *MNRAS*, 318, 753
Gaburov E., Harfst S., Portegies Zwart S., 2009, *New Astron.*, 14, 630
Gieles M., Baumgardt H., 2008, *MNRAS*, 389, L28
Gieles M., Baumgardt H., Heggie D. C., Lamers H. J. G. L. M., 2010, *MNRAS*, 408, L16
Gieles M., Heggie D. C., Zhao H., 2011, *MNRAS*, 413, 2509
Giersz M., Heggie D. C., 1994, *MNRAS*, 268, 257
Giersz M., Heggie D. C., 1997, *MNRAS*, 286, 709
Gnedin O. Y., Ostriker J. P., Tremaine S., 2013, arXiv:1308.0021
Goodman J., 1987, *ApJ*, 313, 576
Harris W. E., Harris G. L. H., Alessi M., 2013, *ApJ*, 772, 82
Heggie D., Hut P., 2003, in Heggie D., Hut P., eds, *The Gravitational Million-Body Problem: A Multidisciplinary Approach to Star Cluster Dynamics*. Cambridge University Press, Cambridge, 372 pp.
Heggie D. C., 1975, *MNRAS*, 173, 729
Heggie D. C., Mathieu R. D., 1986, in Hut P., McMillan S., eds, *Lecture Notes in Physics*, Vol. 267, *The Use of Supercomputers in Stellar Dynamics*, Springer-Verlag, Berlin, p.233
Heggie D. C., Stevenson D., 1988, *MNRAS*, 230, 223
Hénon M., 1961, *Annales d'Astrophysique*, 24, 369; English translation: arXiv:1103.3499

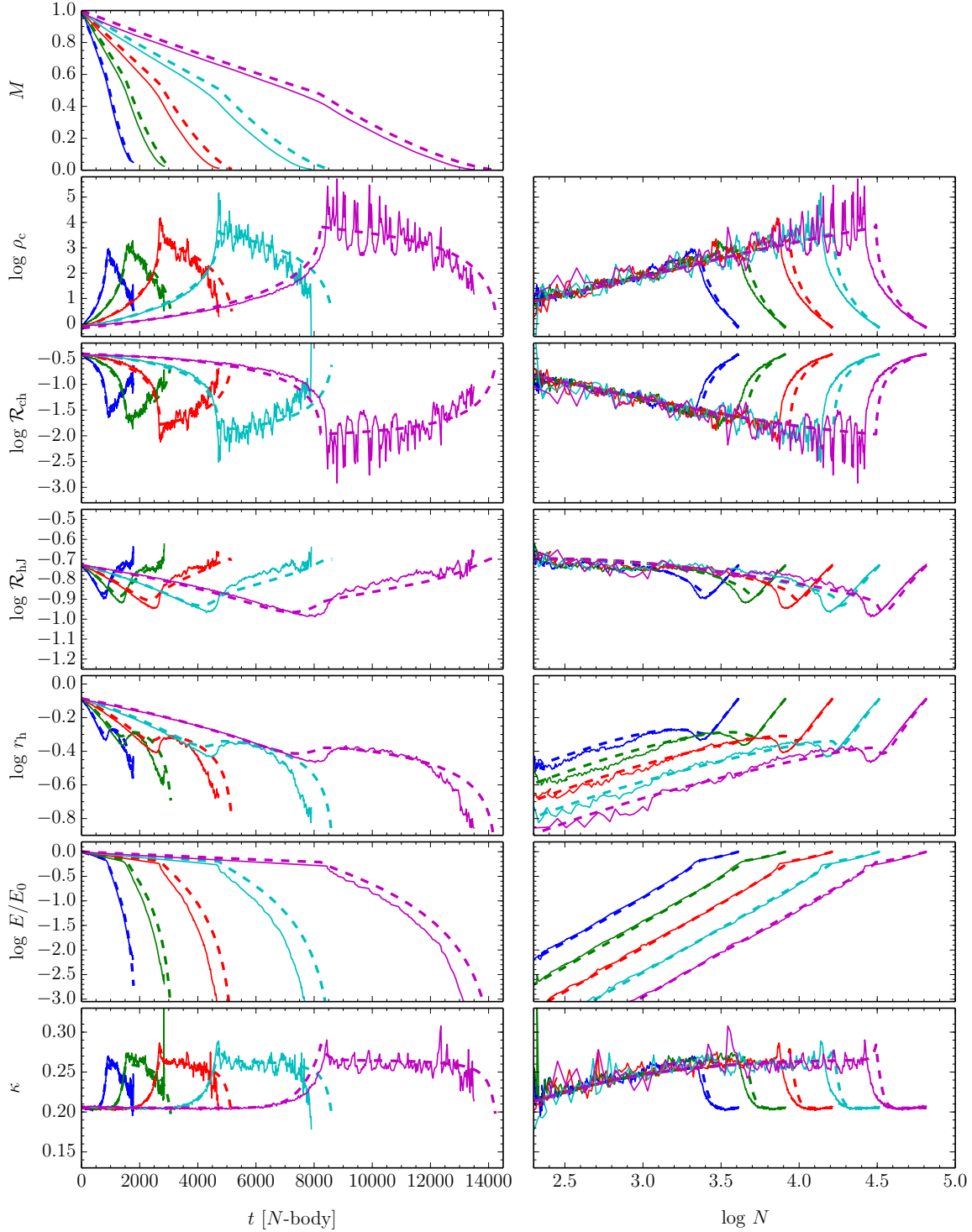


Figure 5. Evolution of all cluster parameters as a function of N -body time (left) and N (right). In the left panels the evolution is from left to right, and in the right-hand panels evolution is from right to left. In the top panel ($M(t)$), the different curves from left to right are for $N = 4\,096$ (blue), $N = 8\,192$ (green), $N = 16\,384$ (red), $N = 32\,768$ and $N = 65\,536$ (magenta). The initial $\mathcal{R}_{hJ} \simeq 1/5$ and the initial conditions for N -body models were given by a King (1966) with $W_0 = 5$. The evolution of all parameters in the unbalanced phase (roughly first half of the evolution) and the balanced phase (roughly second half) is well described by the new version of EMACSS (shown as dashed lines).

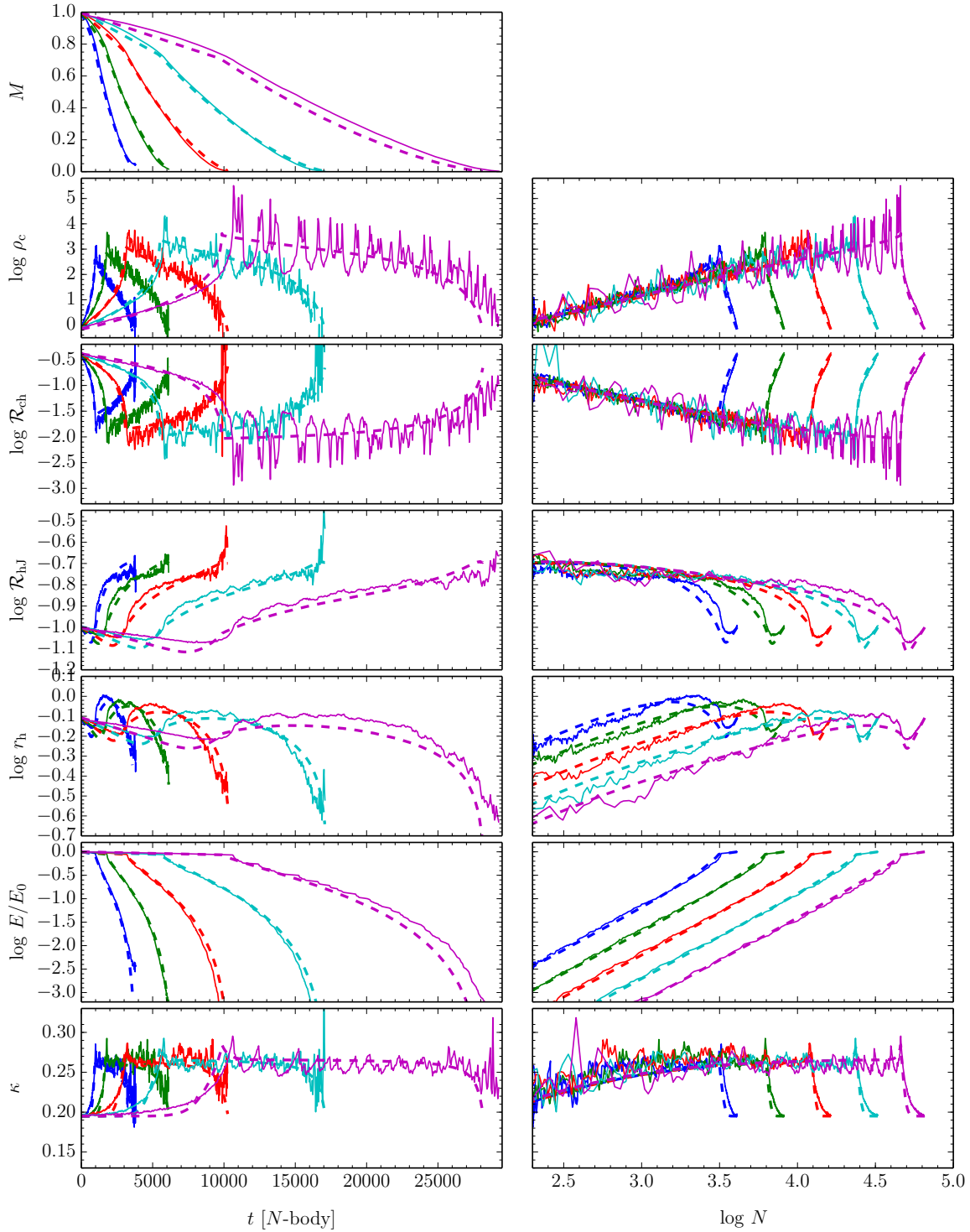


Figure 6. As Fig. 5, but now for $\mathcal{R}_{\text{hJ}}(0) = 1/10$ and a Plummer model as initial conditions. In the left panels the evolution is from left to right, and in the right-hand panels evolution is from right to left.

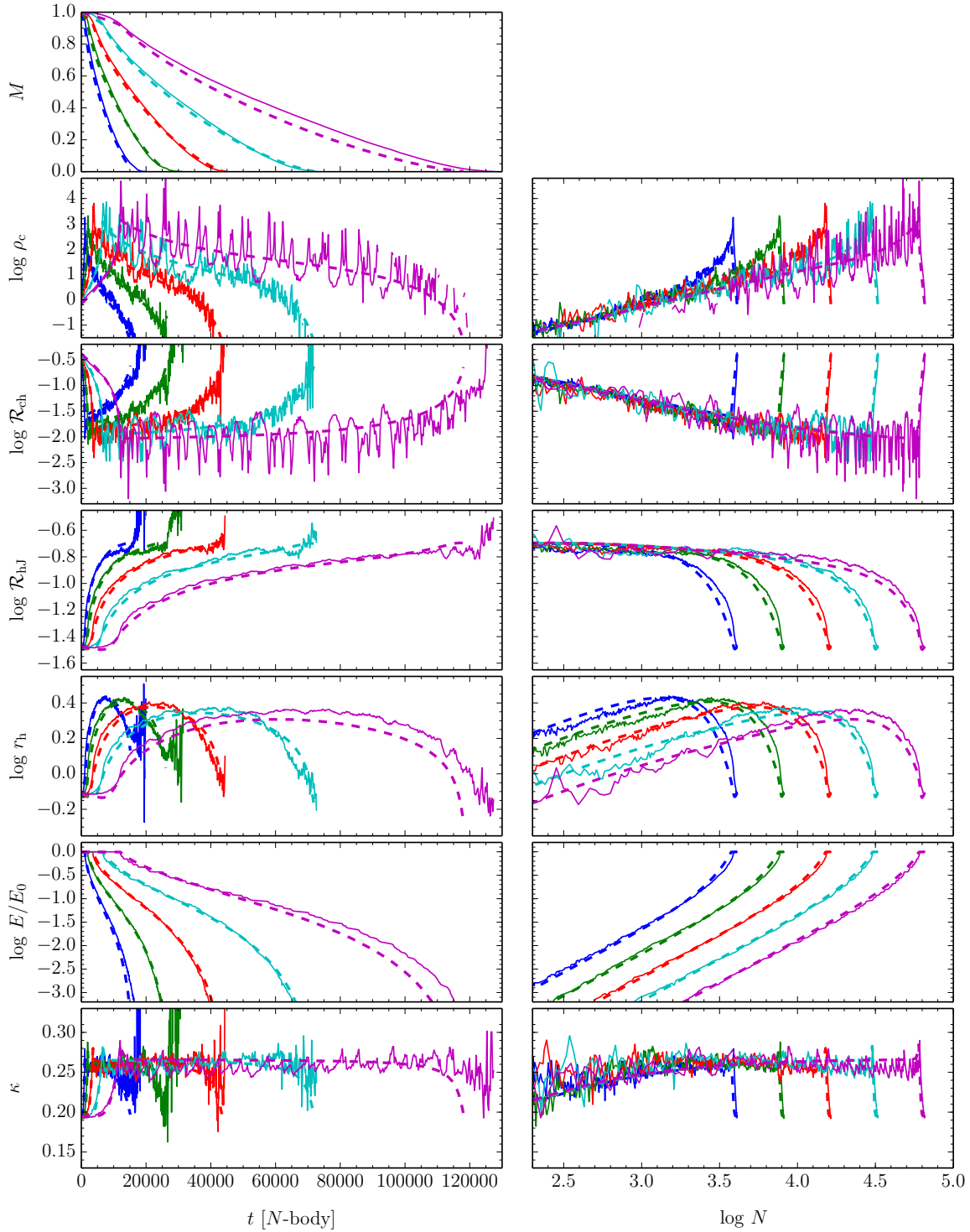


Figure 7. As Fig. 5, but now for $\mathcal{R}_{hJ} = 1/30$ and a Plummer model as initial conditions. In the left panels the evolution is from left to right, and in the right-hand panels evolution is from right to left. These N -body models were first presented in Paper I.

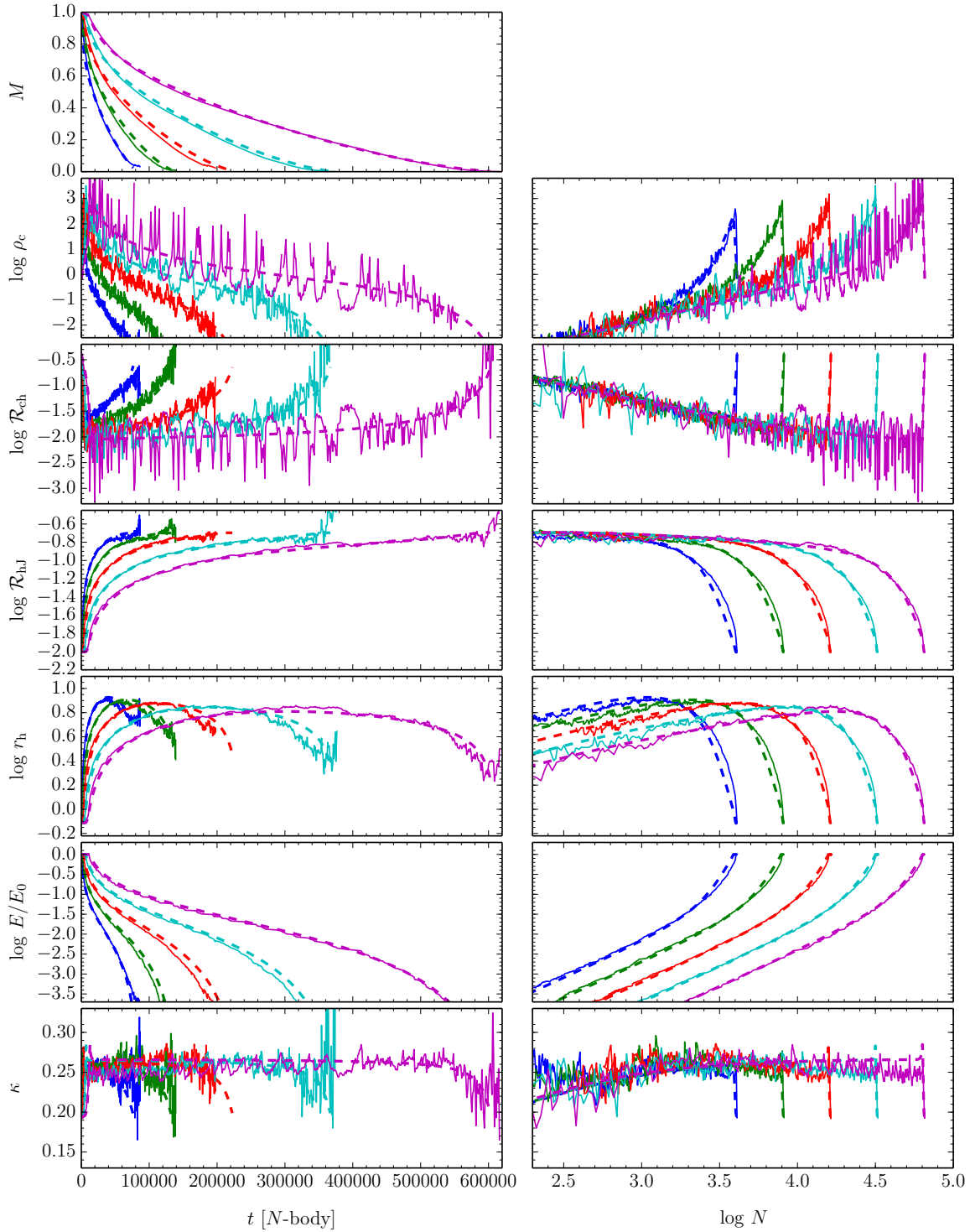


Figure 8. As Fig. 5, but now for $\mathcal{R}_{\text{hJ}} = 1/100$ and a Plummer model as initial conditions. In the left panels the evolution is from left to right, and in the right-hand panels evolution is from right to left. These N -body models were first presented in Paper I.

- Hénon M., 1965, *Annales d'Astrophysique*, 28, 62; English translation: arXiv:1103.3498
- Hurley J. R., Pols O. R., Tout C. A., 2000, *MNRAS*, 315, 543
- Hurley J. R., Shara M. M., 2012, *MNRAS*, 425, 2872
- Hurley J. R., Tout C. A., Pols O. R., 2002, *MNRAS*, 329, 897
- Inagaki S., Lynden-Bell D., 1983, *MNRAS*, 205, 913
- Jordán A., et al., 2005, *ApJ*, 634, 1002
- Jordán A., et al., 2007, *ApJS*, 171, 101
- Kim S. S., Lee H. M., Goodman J., 1998, *ApJ*, 495, 786
- King I. R., 1966, *AJ*, 71, 64
- Lamers H. J. G. L. M., Baumgardt H., Gieles M., 2010, *MNRAS*, 409, 305
- Larson R. B., 1970, *MNRAS*, 150, 93
- Lombardi Jr. J. C., Warren J. S., Rasio F. A., Sills A., Warren A. R., 2002, *ApJ*, 568, 939
- Lynden-Bell D., Eggleton P. P., 1980, *MNRAS*, 191, 483
- Lynden-Bell D., Wood R., 1968, *MNRAS*, 138, 495
- Makino J., Aarseth S. J., 1992, *PASJ*, 44, 141
- Meylan G., Heggie D. C., 1997, *A&AR*, 8, 1
- Nitadori K., Aarseth S. J., 2012, *MNRAS*, 424, 545
- Plummer H. C., 1911, *MNRAS*, 71, 460
- Portegies Zwart S. F., McMillan S. L. W., Gieles M., 2010, *ARA&A*, 48, 431
- Prieto J. L., Gnedin O. Y., 2008, *ApJ*, 689, 919
- Sippel A. C., Hurley J. R., 2013, *MNRAS*, 430, L30
- Spitzer L., 1987, *Dynamical Evolution of Globular Clusters*. Princeton University Press, Princeton, 191 pp.
- Spitzer L. J., Hart M. H., 1971, *ApJ*, 164, 399